Inorganic Chemistry

Article

pubs.acs.org/IC

Improving the Performance of Pt(II) Complexes for Blue Light Emission by Enhancing the Molecular Rigidity

Andreas F. Rausch,[†] Lisa Murphy,[‡] J. A. Gareth Williams,*[,‡] and Hartmut Yersin*[,†]

[†]Institut für Physikalische und Theoretische Chemie, Universität Regensburg, 93053 Regensburg, Germany

[‡]Department of Chemistry, University of Durham, Durham, DH1 3LE, U.K.

ABSTRACT: This study highlights the potential benefits of using terdentate over bidentate ligands in the construction of organometallic complexes as organic light-emitting diode (OLED) emitters offering better color purity, and explores in detail the molecular origins of the differences between the two. A pair of closely related platinum(II) complexes has been selected, incorporating a bidentate and a terdentate cyclometallating ligand, respectively, namely, Pt(4,6-dFppy)(acac) (**1**) {4,6-dFppy = 2-(4,6-difluorophenyl)pyridine metalated at C^2 of the phenyl ring} and Pt(4,6-dFdpyb)Cl (**2**) {4,6-dFdpyb = 4,6-difluoro-1,3-di(2-pyridyl)benzene, metalated at C^2 of the phenyl ring}. The emission properties over the range of temperatures from 1.2 to 300 K have been investigated, including optical high-resolution studies. The results reveal a detailed insight into the electronic and vibronic structures of the two compounds. In particular, the Huang–Rhys parameter S that serves to quantify the degree of molecular distortion in the excited state with respect to the ground state, though small in both cases, is smaller by a factor of 2 for the terdentate than the bidentate complex ($S \approx 0.1$ and ≈ 0.2, respectively). The smaller value for the former reflects the greater degree of rigidity induced by the terdentate ligand, leading to a lesser contribution of intraligand Franck–Condon vibrational modes in the green spectral range of the emission spectra. Consequently, an enhanced color purity with respect to blue light emission results. The high rigidity and the short Pt–C bond in Pt(4,6-dFdpyb)Cl also serve to disfavor nonradiative decay pathways, including those involving higher-lying dd* states. These effects account for the greatly superior luminescence quantum yield of the terdentate complex in fluid solution, amounting to ϕ_{PL} = 80% versus only 2% found for the bidentate complex.

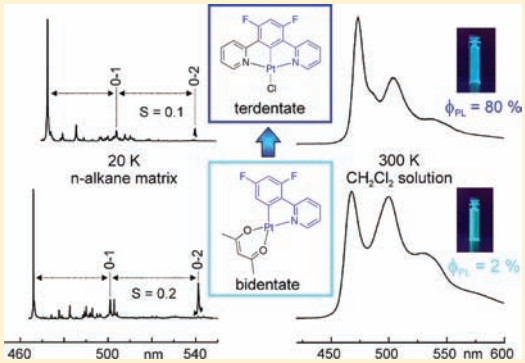

1. INTRODUCTION

In the past decade, organo-transition metal compounds showing efficient phosphorescence at ambient temperature have attracted much attention, driven especially by the applicability of these materials as emitters in organic light-emitting diodes (OLEDs).[1−7] Because of strong spin–orbit coupling (SOC), an internal electroluminescence quantum efficiency of unity can be achieved with such materials, since both the singlet and triplet excitons generated by electron–hole recombination (of which the proportions are 1:3) can be induced to emit (triplet harvesting).[8−10]

Many efficient green- and red-emitting organo-transition metal compounds have been discovered. However, materials exhibiting blue phosphorescence of high quantum yield, and with a color purity sufficient for device applications, are still rare. Nonradiative deactivation via higher-lying metal-centered dd* states,[11−13] and even degradation due to bond-breaking processes,[11,14] become important competitive pathways as the excited-state energy increases to that required for good blue emission. Both mechanisms are consequences of the population of highly antibonding metal d*-orbitals, which can lead to severe geometrical distortions of the molecules.[15]

Strategies to achieve blue emission and to avoid these problems make use of, for example, C^C coordinating carbenes,[16−18] N^C coordinating phenyltriazolates,[19] or N^N coordinating pyridylpyrazolates[20] and pyridyltriazolates[21] as chromophoric ligands. Alternative approaches focus on ancillary ligands with high ligand-field strengths, such as CO, CN^-,[22−24] or pyrazolylborates.[25] Very recently, efficient blue-light emission has been realized with Cu(I) complexes.[13,26]

Currently, most blue-emitting materials are based on Ir(III) as the central metal ion. On the other hand, a number of Pt(II) compounds that exhibit blue phosphorescence are also known.[18,27−29] These materials offer additional possibilities for light generation, since their square-planar coordination geometry favors intermolecular interactions in concentrated solutions, doped films, or neat samples, leading to excimers[30−32] or aggregates.[33−36] Such interacting species may themselves display efficient emission, which usually is broad and red-shifted with respect to the monomer emission. A balanced combination of blue-green monomer and yellow-to-red aggregate/excimer emission can be utilized for the generation of white electroluminescence using a single dopant material.[37−40]

Received: August 2, 2011
Published: November 30, 2011

dx.doi.org/10.1021/ic201664v | *Inorg. Chem.* 2012, 51, 312–319

In 2002, a series of heteroleptic Pt(II) compounds based on N^C-coordinating phenylpyridine-type ligands were reported, several of them showing blue monomer emission.[28] However, these complexes exhibit only relatively low quantum efficiencies in fluid solutions at ambient temperature and, despite the high energy of the emitting triplet state T_1, not a deep blue but a turquoise luminescence due to intense vibrational satellite bands in the green spectral range. A representative example is Pt(4,6-dFppy)(acac) (**1**) (for photophysical studies of this compound see refs 41−43). On the other hand, it has been reported that complexes of terdentate, N^C^N-coordinating dipyridylbenzene (dpyb) ligands exhibit significantly higher quantum yields when compared to related materials with bidentate N^C-coordinating ligands.[31,44,45] Pt(dpyb)Cl itself is a highly efficient green emitter (ϕ_{PL} = 0.60 in deoxygenated CH_2Cl_2 at 298 K).[44] As for the bidentate class, introduction of electron-withdrawing substituents, such as fluorine, into the central phenyl ring of the terdentate ligand, *meta* to the C−Pt bond, significantly increases the T_1 state energy, allowing blue-emitting materials to be obtained.[29,46] Pt(dpyb)Cl and its derivatives have also been studied theoretically[47−49] and have been applied, for example, as OLED emitters,[50,51] sensors for oxygen[52] and metal ions,[53] and in time-resolved live-cell imaging.[54]

In this work, we present a detailed comparative study of the blue light-emitting terdentate Pt(4,6-dFdpyb)Cl (**2**), and the structurally related bidentate Pt(4,6-dFppy)(acac) (**1**) (Figure 1). Beside investigations of emission properties at ambient temperature and at 77 K, techniques of high-resolution laser spectroscopy at cryogenic temperatures were applied to gain information on the electronic structures of the emitting triplet states, the zero-field splittings, and the individual decay times of the T_1 sublevels of both materials. This allows us to evaluate the efficiency of SOC.[13,41] Furthermore, we will focus on the color purity of blue light emission and elucidate how this is related to the different molecular structures of the materials, which significantly affect the couplings of intraligand vibrational modes to the purely electronic transitions. The intensities of the resulting Franck−Condon induced vibrational satellites, which are related to the so-called Huang−Rhys parameters, crucially determine the color of the emitted light both at cryogenic temperatures and at 300 K. Moreover, we also consider differences in the radiative and nonradiative deactivation processes of the two compounds, since their suitability for OLED applications is strongly related to the emission quantum yields.

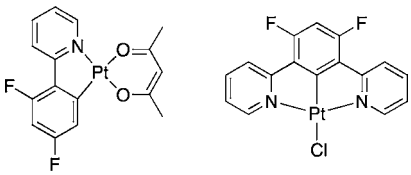

Figure 1. Structures of Pt(4,6-dFppy)(acac) (**1**) and Pt(4,6-dFdpyb)-Cl (**2**).

2. EXPERIMENTAL SECTION

Pt(4,6-dFdpyb)Cl was synthesized according to the procedures described in refs 31 and 44, and Pt(4,6-dFppy)(acac) as reported in ref 28.

For spectroscopic measurements at 300 K, the compounds were dissolved in CH_2Cl_2 at a concentration of about 10^{-5} mol/L. Doped PMMA films were prepared by dissolving the compounds (≈ 1 weight-%) together with PMMA in CH_2Cl_2. Subsequently, the solutions were spin-coated on a quartz plate. Absorption spectra were recorded with a Varian Cary 300 double beam spectrometer. Emission spectra at 300 and 77 K were measured with a steady-state fluorescence spectrometer (Jobin Yvon Fluorolog 3). Absolute luminescence quantum yields were determined with a commercially available system using an integrating sphere (Hamamatsu Photonics C9920-02). The estimated relative error of the quantum yields is about 10%. Fluid solutions were degassed by at least three freeze−pump−thaw cycles with a final vapor pressure at 77 K of ≈10^{-5} mbar. A pulsed diode laser (PicoQuant PDL 800-B) with an excitation wavelength of 372 nm and a pulse width of about 500 ps or a pulsed Nd:YAG laser (IB Laser Inc., DiNY pQ 02) with a pulse width of about 7 ns, using the third harmonic at 355 nm, were applied as excitation sources for lifetime measurements. Decay times were registered using a FAST Comtec multichannel scaler PCI card with a time resolution of 250 ps.

For investigations at cryogenic temperatures, Pt(4,6-dFppy)(acac) (**1**) and Pt(4,6-dFdpyb)Cl (**2**) were dissolved in *n*-octane and *n*-decane, respectively, at concentrations of about 5 × 10^{-6} mol/L. The measurements were carried out in a helium cryostat (Cryovac Konti Cryostat IT), in which the heating, the He gas flow, and the pressure were controlled. Magnetic-field experiments were performed in an Oxford Instruments MD10 cryostat equipped with a 12 T magnet. For recording site-selective emission and excitation spectra, a pulsed dye laser (Lambdaphysik Scanmate 2C) pumped by a frequency-tripled Nd:YAG laser was operated. The spectra were measured with an intensified CCD camera (Princeton PIMAX) or with a cooled photomultiplier (RCA C7164R) attached to a triple spectrograph (S&I Trivista TR 555).

3. RESULTS AND DISCUSSION

3.1. Photophysical Properties at Room Temperature.

The absorption spectra of Pt(4,6-dFppy)(acac) (**1**) and Pt(4,6-dFdpyb)Cl (**2**) in CH_2Cl_2 at ambient temperature are shown in Figure 2. For both compounds, intense absorptions below 300 nm ($\varepsilon > 10^4$ M^{-1} cm^{-1}) can be assigned to transitions to singlet states which are largely centered at the chromophoric ligands 4,6-dFppy or 4,6-dFdpyb (^{1}LC states).[27,41,44] The bands at lower energy are absent in the absorption spectra of the free ligands, indicating that they represent transitions to states with metal-to-ligand charge-transfer (MLCT) parentage.

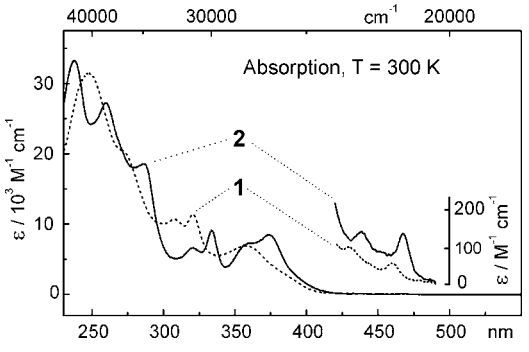

Figure 2. Absorption spectra of Pt(4,6-dFppy)(acac) (**1**) (dashed lines) and Pt(4,6-dFdpyb)Cl (**2**) (solid lines) dissolved in CH_2Cl_2 (c ≈ 10^{-5} mol/L) at 300 K.

dx.doi.org/10.1021/ic201664v | *Inorg. Chem.* 2012, 51, 312−319

At wavelengths above ≈425 nm, weak absorptions from the ground state to the lowest triplet states can be observed for both compounds. For Pt(4,6-dFppy)(acac) (**1**), the electronic $S_0 \rightarrow T_1$ transition lies at 459 nm (21790 cm^{-1}, ε = 90 M^{-1} cm^{-1}) and for Pt(4,6-dFdpyb)Cl (**2**) at 467 nm (21410 cm^{-1}, ε = 140 M^{-1} cm^{-1}). The higher extinction coefficient for the singlet → triplet absorption of **2** already indicates that SOC to higher lying ^{1}MLCT states is slightly more effective in the terdentate compound.

Figure 3 shows normalized emission spectra of **1** and **2** at ambient temperature in deaerated CH_2Cl_2 solution (compare also ref 27). Both spectra are structured; the high-energy emission maxima corresponding to the respective electronic $T_1 \rightarrow S_0$ transitions lie at 467 nm (**1**) and at 472 nm (**2**), respectively. The Stokes shift of ≈250 cm^{-1} for the terdentate compound is significantly smaller than for the bidentate complex, for which the corresponding shift is about 400 cm^{-1}. The smaller Stokes shift found for **2** may be ascribed to the higher molecular rigidity of Pt(4,6-dFdpyb)Cl as compared to Pt(4,6-dFppy)(acac).

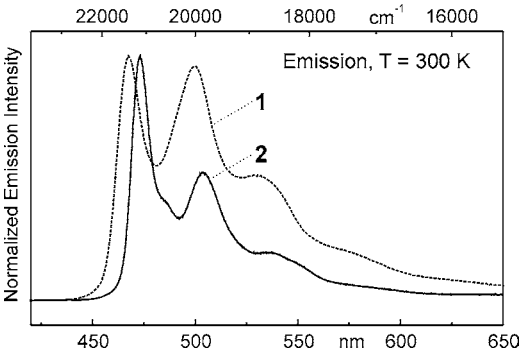

Figure 3. Emission spectra of Pt(4,6-dFppy)(acac) (**1**) (λ_{exc} = 360 nm, dashed line) and Pt(4,6-dFdpyb)Cl (**2**) (λ_{exc} = 370 nm, solid line) dissolved in CH_2Cl_2 ($c \approx 10^{-5}$ mol/L) at ambient temperature.

The intensities of the bands at lower energy, corresponding to vibrational satellites of ground state modes as well as to combinations and/or progressions of these modes, are distinctly lower for Pt(4,6-dFdpyb)Cl than for Pt(4,6-dFppy)(acac). This has important consequences for the color of the emitted light. Thus, despite the high emission energy of the electronic $T_1 \rightarrow S_0$ transition, lying in the deep blue spectral range, Pt(4,6-dFppy)(acac) exhibits a turquoise luminescence due to the contribution of these intense vibrational bands in the green spectral range. The corresponding (*x*; *y*) CIE color coordinates[55] are (0.22; 0.41). For Pt(4,6-dFdpyb)Cl, the intensities of the low-energy vibrational bands as compared to the intensity of the electronic origin are much smaller and thus a sky-blue emission results (CIE coordinates: 0.18; 0.38), even though the electronic $T_1 \rightarrow S_0$ transition actually lies at a longer wavelength than that of Pt(4,6-dFppy)(acac). These color differences are also related to the different molecular structures (rigidities) of the two compounds; a detailed discussion follows below. For completeness, it may be noted that, apart from a very slight blue shift of ≈2 nm, the emission spectra of both materials when doped into a PMMA (polymethylmethacrylate) host are essentially identical to those in fluid CH_2Cl_2.

The emission properties of Pt(4,6-dFppy)(acac) and Pt(4,6-dFdpyb)Cl at ambient temperature are summarized in Table 1. Pt(4,6-dFdpyb)Cl is highly emissive in deaerated CH_2Cl_2 solution, exhibiting a quantum yield ϕ_{PL} of 0.80 and a decay time of 6.4 μs. In contrast, the phosphorescence quantum yield of Pt(4,6-dFppy)(acac), ϕ_{PL} = 0.02, is very low and the decay time of 250 ns is very short.[28,41] Evidently, this behavior can be ascribed to a high nonradiative decay rate. Because of the high emission energy, both the quantum efficiency and the decay time of Pt(4,6-dFppy)(acac) in fluid solution are severely reduced by the thermally activated population of a relatively close-lying dd* state, which is strongly distorted with respect to the ground state and undergoes efficient radiationless decay.[28,41] On the other hand, as discussed below, the activation energy of a corresponding state in Pt(4,6-dFdpyb)Cl is significantly higher, reducing its thermal population at 300 K. As a consequence, a high quantum yield in fluid ambient temperature solution results. A dominant reason for the distinctly higher activation energy in Pt(4,6-dFdpyb)Cl is likely to be the significantly shorter platinum−carbon bond of ≈1.91 Å[46] as compared to ≈2.0 Å[56] in the bidentate compound. Consequently, a higher ligand-field strength results for the N^C^N ligand, which destabilizes the quenching metal-centered states. Additionally, the T_1 state of the terdentate compound lies about 250 cm^{-1} lower than that of the bidentate material, which will also contribute to a reduction of the quenching efficiency of dd* states in **2**.

Table 1. Emission Properties of Pt(4,6-dFppy)(acac) (1) and Pt(4,6-dFdpyb)Cl (2) at Ambient Temperature in CH_2Cl_2 and Doped into PMMA

	Pt(4,6-dFppy)(acac) (**1**)		Pt(4,6-dFdpyb)Cl (**2**)	
	CH_2Cl_2	PMMA	CH_2Cl_2	PMMA
λ_{max} [nm]	467	465	472	473
τ_{em} [μs]	0.25	5.3	6.4	6.3
ϕ_{PL}	0.02	0.50	0.80	0.85
k_r^a [s^{-1}]	7.7×10^4	7.0×10^4	1.2×10^5	1.3×10^5
k_{nr}^a [s^{-1}]	3.8×10^6	7.0×10^4	3.6×10^4	2.5×10^4
CIE coordinates (x; y)	0.22; 0.41		0.18; 0.38	

[a]Radiative and nonradiative rate constants are calculated from the quantum yields and emission decay times according to $\phi_{PL} = k_r \cdot \tau_{em} = k_r/(k_r + k_{nr})$.

Moreover, the emission properties are crucially determined by the different molecular rigidities of the compounds. Unlike the relatively rigid Pt(4,6-dFdpyb)Cl, Pt(4,6-dFppy)(acac) can more easily undergo geometrical distortions upon excitation such as bond elongations or torsional distortions away from square planarity toward a tetrahedral symmetry, at least in "soft" fluid solution. This can lead to a stabilization of the dd* state(s) and consequently further increase their thermal population. However, in a more "rigid" environment, like in a PMMA host, such distortions or related energy stabilizations of the quenching states are largely prevented or are at least less distinct. Consequently, the nonradiative decay rate of the bidentate compound is much smaller in PMMA than in fluid solution and a distinctly higher emission quantum yield of ϕ_{PL} = 0.5 is found. Similar models have also been applied to explain the relatively high emission quantum yields of Ru(II) polypyridine compounds in rigid host media, such as zeolites,[57] glasses,[58] or polymeric matrixes[59] when compared with fluid solutions. For Pt(4,6-dFdpyb)Cl, being intrinsically more rigid, these effects are less important, since the excited molecule is much less affected by geometrical distortions and stabilizations of the quenching dd* states. Thus, the emission quantum yield

dx.doi.org/10.1021/ic201664v | Inorg. Chem. 2012, 51, 312−319

is only slightly different if measured in fluid solution (0.80) as compared to PMMA (0.85) (Table 1).

The radiative rate constants of the compounds at ambient temperature are nearly independent of the host environment, with that of Pt(4,6-dFdpyb)Cl (**2**) being higher than that of Pt(4,6-dFppy)(acac) (**1**). This is in accordance with the higher extinction coefficient of the electronic $S_0 \rightarrow T_1$ transition found for **2** than for **1** (see Figure 2) and supports the assumption of stronger SOC in the terdentate compound. However, a more detailed understanding of the influence of SOC on the photophysical properties of the materials is not feasible on the basis of the broad and relatively unresolved spectra measured at ambient temperature. Therefore, we decided to make a comparative study of the two complexes with methods of high-resolution optical spectroscopy at cryogenic temperatures. This procedure will allow us to gain a deeper insight into the properties of the emitting triplet states.[41,60−62]

3.2. Vibrational Satellite Structures and Excited State Distortions. For studies at liquid helium temperatures, the compounds were dissolved in *n*-alkanes at low concentration and rapidly cooled. In the polycrystalline alkane matrixes, the guest molecules (dopants) substitute host molecules and thus lie at defined positions. In suitable cases, the application of the so-called Shpol'skii[63] or matrix isolation technique results in highly resolved spectra with line widths of only a few cm^{-1}.[35,41,42,45,60,62] These widths are smaller, by a factor of the order of 100, than those usually obtained with amorphous or glassy host materials. The resulting spectra mostly represent superpositions of spectra that stem from different sites, corresponding to dopant molecules with slightly different local environments in the polycrystalline host. However, using a tunable dye laser, one specific site can be excited selectively and studied individually.

Figures 4 and 5 show the emission spectra of Pt(4,6-dFppy)(acac) (**1**) and Pt(4,6-dFdpyb)Cl (**2**) at different temperatures in *n*-octane and *n*-decane, respectively. These

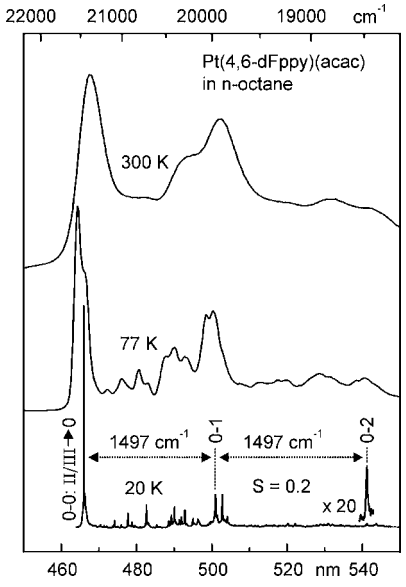

Figure 4. Emission spectra of Pt(4,6-dFppy)(acac) (**1**) in *n*-octane at various temperatures. The excitation wavelengths were 360 nm for the 300 and 77 K spectra, and 451.12 nm (22167 cm^{-1}, 0−0 transition 0 → II/III + vibrational energy of 706 cm^{-1}) for the selectively excited 20 K spectrum.

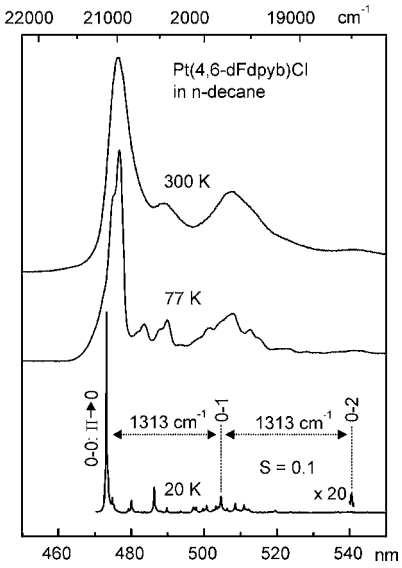

Figure 5. Emission spectra of Pt(4,6-dFdpyb)Cl (**2**) in *n*-decane at various temperatures. The excitation wavelengths were 375 nm for the 300 and 77 K spectra, and 454.52 nm (22001 cm^{-1}, 0−0 transition 0 → II + vibrational energy of 866 cm^{-1}) for the selectively excited 20 K spectrum.

hosts proved to be most suited for the respective compounds. For both materials, the emission spectra at ambient temperature are similar to those measured in CH_2Cl_2 and depicted in Figure 3. However, because of the much lower polarity of the *n*-alkanes, some additional structures are resolved. In the 77 K spectra, this effect is even more pronounced. The improvement of resolution becomes drastic when the samples are cooled with liquid helium. For example, the selectively excited emission spectra at 20 K show a series of narrow lines with halfwidths of only a few cm^{-1}. Contributions of dopant molecules located in other sites, or of inhomogeneously distributed emitter molecules, can largely be neglected.

For both compounds, an intense high-energy line can be observed, representing the respective 0−0 transitions from the higher-lying T_1 substates II (and III) to the singlet ground state S_0. This will be discussed in more detail in section 3.3. The lines of minor intensity at lower energy correspond to vibrational satellites involving ground state modes, which couple to the purely electronic transitions II → 0 and III → 0. Low energy modes (with energies up to ≈100 cm^{-1} relative to the electronic 0−0 transition) are largely determined by vibrations of the dopant in its matrix cage, representing so-called local phonon modes.[64,65] Overlapping with this energy range up to about 600 cm^{-1}, metal−ligand (M-L) vibrations are found,[62,66] while fundamentals higher than ≈600 cm^{-1} can usually be assigned to internal ligand modes.[61,62,67,68] For the most intense satellites, second members of progressions can be observed for both compounds. Representative satellites of the intraligand modes with vibrational energies of 1497 cm^{-1} {for Pt(4,6-dFppy)(acac)} and 1313 cm^{-1} {for Pt(4,6-dFdpyb)Cl} are marked in Figures 4 and 5, respectively. The occurrence of progressions clearly shows that these vibrational modes stem from Franck−Condon activity.[62,69,70] Presumably, this is also valid for all other fundamental modes that are prominent in the 20 K spectra. However, because of the low intensities of most fundamental satellites, the second members of the Franck−

dx.doi.org/10.1021/ic201664v | *Inorg. Chem.* 2012, 51, 312−319

Condon progressions are too weak to be distinguished from the spectral background.

For those modes showing second members of vibrational progressions, one can determine the so-called Huang–Rhys parameter S, which is specific for each vibrational mode and depends on the shift ΔQ of the equilibrium positions of the involved electronic states for the corresponding vibrational coordinate.[62,69,70] For example, a Huang–Rhys parameter of zero would correspond to equal geometries of the excited state and the ground state. In this case, the whole emission intensity is carried by the electronic 0–0 transition. With an increase of the displacement ΔQ and thus an increase of S, the intensity of the electronic 0–0 line decreases and the vibrational satellites of the respective Franck–Condon progression grow in. In the low-temperature limit, the Huang–Rhys parameter for a specific Franck–Condon progression does not depend on the vibrational energy and can be determined by using the simple expression[62,69,71]

$$S = v \cdot \frac{I_v}{I_{v-1}} \quad (1)$$

wherein v is the vibrational quantum number and I_v is the intensity of the respective progression member.

At T = 20 K, the Huang–Rhys parameter for the most intense fundamentals of Pt(4,6-dFppy)(acac) amounts to $S \approx 0.2$, which is depicted for the 1497 cm^{-1} intraligand mode in Figure 4. Interestingly, the maximum Huang–Rhys parameter for the vibrational modes of Pt(4,6-dFdpyb)Cl at 20 K is only half as large and amounts to $S \approx 0.1$, as shown for the 1313 cm^{-1} fundamental (Figure 5). Values of that magnitude show that, for both compounds, only very small geometry changes between the singlet ground state and the emitting T_1 state occur, at least in the rigid n-alkane matrixes at cryogenic temperatures. However, the decrease from 0.2 to 0.1, being as large as 50%, is enormous and can be ascribed to the different structures of the two compounds. In the Pt(N^C) system, the displacements ΔQ of the potential energy surfaces of the involved states along the vibrational coordinate of the corresponding high-energy intraligand modes are evidently larger than in the rigid Pt(N^C^N) system.

With temperature increase from 20 to 77 K and then to 300 K, the spectral resolution is lost and the vibrational satellites strongly overlap (Figures 4 and 5). Consequently, "exact" Huang–Rhys parameters for specific modes cannot be determined any more. However, the spectra clearly show that the intensities of the vibrational satellite bands relative to the electronic origin become distinctly larger with increasing temperature. In principal, the temperature dependence of Huang–Rhys parameters can be considered by introducing a so-called effective Huang–Rhys parameter,[70] since eq 1 is strictly valid only for a temperature of 0 K. However, for high-energy vibrations, the temperature dependence of S is negligibly small. For example, for a vibrational mode with an energy of 1500 cm^{-1}, a low-temperature Huang–Rhys parameter of 0.1 increases only marginally to 0.1001 at 300 K. Thus, the observed temperature dependent intensity increase of the vibrational bands has another origin. Most likely, the n-alkane matrixes become less rigid with increasing temperature. Presumably, this is related to an anisotropic increase of the cell parameters, as suggested in ref 72. At 300 K in a "soft" fluid environment, an even more pronounced displacement of the involved potential energy surface upon excitation is possible. As a consequence, the Huang–Rhys parameters further increase, and the vibrational bands become more intense (compare Figures 4 and 5).

Interestingly, the trends observed at 20 K are also reflected in the emission spectra at 77 K and at 300 K. In particular, for Pt(4,6-dFdpyb)Cl, the intensities of the overlapping vibrational satellite bands (as compared to the electronic origin) are significantly weaker than for Pt(4,6-dFppy)(acac). Consequently, the much better color purity of the terdentate compound with respect to blue emission, as discussed in section 3.1, is largely independent of temperature.

3.3. Electronic Structures of the Emitting Triplet States. In this section, we focus on the electronic 0–0 transitions between the T_1 substates and the singlet ground state S_0. Figures 6 and 7 show site-selective emission and excitation spectra of Pt(4,6-dFppy)(acac) (**1**) in n-octane and Pt(4,6-dFdpyb)Cl (**2**) in n-decane in the range of the electronic origins at different conditions. For both materials, the three substates of the emitting triplet state T_1 can be identified.

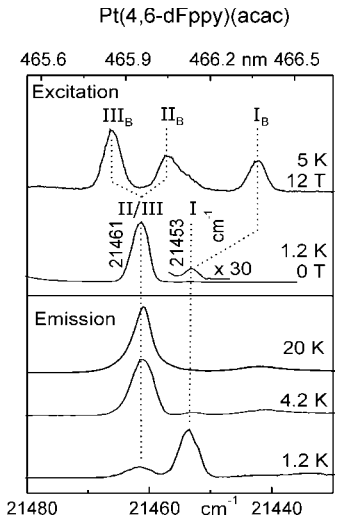

Figure 6. Site-selective excitation and emission spectra of Pt(4,6-dFppy)(acac) (**1**) in n-octane at different temperatures and magnetic fields in the range of the electronic 0–0 transitions ($T_1 \leftrightarrow S_0$ transitions). Detection energy for the excitation spectra: 21012 cm^{-1} (I → 0–441 cm^{-1}, T = 1.2 K, B = 0 T) and 20723 cm^{-1} (III_B → 0–743 cm^{-1}, T = 5 K, B = 12 T). Excitation energy for the emission spectra: 22167 cm^{-1} (0 → II/III + 706 cm^{-1}). The index B denotes transitions which are shifted by the applied magnetic field. (Compare refs 42, 43.).

For Pt(4,6-dFppy)(acac) in n-octane, only two lines corresponding to electronic 0–0 transitions can be observed in excitation and emission at zero magnetic field, lying at 21453 and 21461 cm^{-1}, respectively (Figure 6). The high-energy transition carries a distinctly higher oscillator strength. Applying a high magnetic field, the line at 21461 cm^{-1} splits into two lines, as depicted in the excitation spectrum at B = 12 T. Thus, it follows that the substates II and III are almost energetically degenerate with respect to our experimental resolution at zero magnetic field and therefore are hidden under one line.[42,43] In summary, the zero-field splitting of Pt(4,6-dFppy)(acac) in n-octane amounts to $\Delta E_{II-I} \approx \Delta E_{III-I} = \Delta E(ZFS) = 8.3$ cm^{-1}.

Pt(4,6-dFdpyb)Cl allows us to observe all three triplet substates in excitation; the lines lie at 21129 (0 → I), 21135 (0 → II), and 21140 cm^{-1} (0 → III), respectively (Figure 7). An

dx.doi.org/10.1021/ic201664v | Inorg. Chem. 2012, 51, 312–319

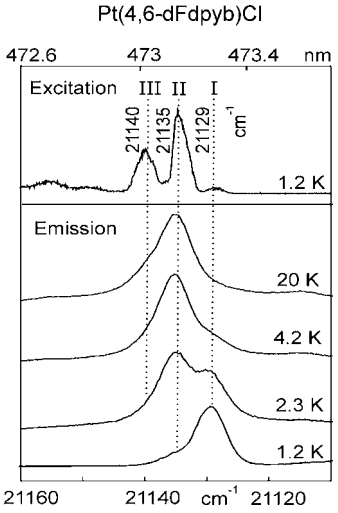

Figure 7. Site-selective excitation and emission spectra of Pt(4,6-dFdpyb)Cl (**2**) in *n*-decane at different temperatures in the range of the electronic 0−0 transitions ($T_1 \leftrightarrow S_0$ transitions). Detection energy for the excitation spectrum: 20681 cm^{-1} (I → 0−448 cm^{-1}). Excitation energy for the emission spectra: 22001 cm^{-1} (0 → II + 866 cm^{-1}).

intensity ratio of Int(0 → II)/Int(0 → III)/Int(0 → I) = 15/10/1 is found, which displays the ratio of the oscillator strengths (allowednesses) of the corresponding transitions. According to its low allowedness, the very weak transition I → 0 can be observed in emission only at low temperatures below 4.2 K. At higher temperature, emission from substate II dominates, while the 0−0 transition III → 0 occurs, because of its somewhat lower allowedness, only as a shoulder. The spectra depicted in Figure 7 allow us to determine the zero-field splitting parameters of Pt(4,6-dFdpyb)Cl in *n*-decane to be ΔE_{II-I} = 5.8 cm^{-1} and ΔE_{III-I} = ΔE(ZFS) = 11.3 cm^{-1}.

Temperature dependent measurements of the thermalized emission decay time provide additional information. Such studies are well-established in the literature and can be applied to determine the decay times of the individual T_1 substates by fitting a Boltzmann-weighted function for the depopulation of the three thermally equilibrated sublevels to the emission decay time at different temperatures (see, for example, refs 41, 73, 74, and 75 for details of this approach). For both compounds, the zero-field splitting parameters, which are known from highly resolved spectra as discussed above, were kept fixed during the fitting procedure.[76] The resulting decay times of the individual T_1 substates and the zero-field splitting parameters are summarized in the energy level diagrams shown in Figure 8 (compare also refs 41, 42). For both compounds, the substates II and III exhibit distinctly shorter individual decay times than substate I, showing that the respective transitions from the higher lying substates to the singlet ground state carry distinctly more allowedness than the transition from substate I.

4. ASSIGNMENTS AND CONCLUSION

A comparison of the triplet state properties of Pt(4,6-dFppy)(acac) and Pt(4,6-dFdpyb)Cl reveals total zero-field splittings of ΔE(ZFS) = 8.3 and 11.3 cm^{-1}, respectively. According to an empirical ordering scheme,[9,13,41,60] which relates the magnitude of ΔE(ZFS) to the orbital nature of the emitting triplet state, the T_1 states of both compounds can be classified as largely ligand centered (LC) states with moderate

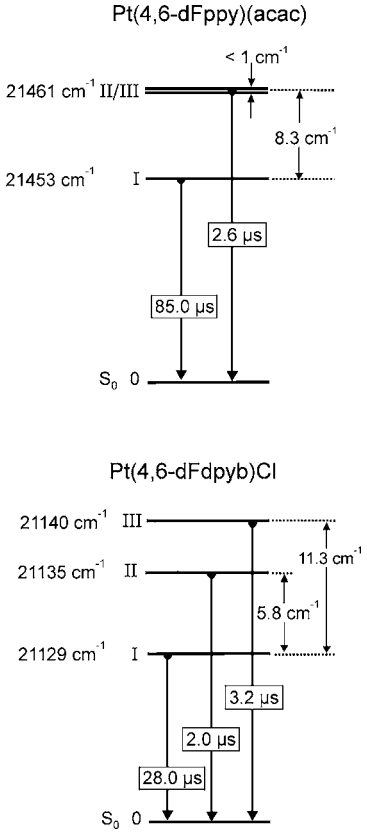

Figure 8. Energy level diagrams of the emitting triplet states and individual emission decay times of the T_1 substates of Pt(4,6-dFppy)(acac) (**1**) in *n*-octane (top, adapted from refs 42, 43) and Pt(4,6-dFdpyb)Cl (**2**) in *n*-decane (bottom).

metal-to-ligand charge-transfer (MLCT) admixtures. The MLCT contributions are displayed in distinct $S_0 \rightarrow T_1$ absorptions (Figure 2) and are in accordance with the relatively short individual decay times of the higher lying T_1 substates II and III, which mainly govern the emission properties at ambient temperature. It has been derived that emitting states that are largely of ^{3}LC character cannot couple via direct SOC to higher lying singlet and triplet MLCT states.[13,41,77] However, an admixture of such states to the T_1 state is obviously present. A corresponding coupling can proceed via a two-step mechanism involving configuration interaction of the ^{3}LC substates with the substates of higher lying ^{3}MLCT states. The latter can mix via direct SOC with other ^{1,3}MLCT states, which, however, have to involve different central-metal d-orbitals (for details see refs 13, 41, 60, 77, 78).

On the other hand, a comparison of the total zero-field splittings indicates that the ΔE(ZFS) of 11.3 cm^{-1} for Pt(4,6-dFdpyb)Cl is about 40% larger than the value of 8.3 cm^{-1} for Pt(4,6-dFppy)(acac). Interestingly, this trend is also reflected in the averaged radiative decay rate determined at ambient temperature, which is larger for the former compound (Table 1). However, the distinctly higher quantum yield of the terdentate material in fluid solution is mainly a consequence of the significantly lower nonradiative rates as discussed in section 3.1. In summary, it can be concluded that SOC to both singlet and triplet MLCT states (via configuration interaction) is slightly more effective in the terdentate than in the bidentate complex. In particular, the singlet admixtures govern the radiative rates, while the ^{3}MLCT contributions probably mainly

dx.doi.org/10.1021/ic201664v | Inorg. Chem. 2012, 51, 312−319

cause different energy stabilizations of the three substates, leading to the zero-field splitting.[13,41,60]

In conclusion, the drastic photophysical differences between the two studied compounds can be mainly traced back to the different molecular rigidities. Pt(4,6-dFdpyb)Cl exhibits a less pronounced distortion of the molecular geometry in the emitting triplet state with respect to the singlet ground state than Pt(4,6-dFppy)(acac). As a consequence, Franck−Condon activity is higher for the bidentate compound. This behavior can be quantified by the observed Huang−Rhys parameters, which govern the intensities of the low-energy vibrational satellite bands.

Moreover, the distinctly shorter Pt−C bond length observed for Pt(4,6-dFdpyb)Cl than for Pt(4,6-dFppy)(acac) results in a higher ligand field strength for the former compound. Thus, the activation energy for quenching via metal centered dd* states increases. Together with the higher rigidity of the terdentate compound, preventing distortions and bond elongations even in "soft" environments like fluid solutions, this effect is responsible for the drastically higher emission quantum yield at ambient temperature for the terdentate emitter. In a rigid PMMA host, a medium more relevant to OLED applications and which also contributes to suppress geometrical distortions of the dopants upon excitation, the differences in the emission quantum yields between the two compounds are less pronounced. However, the terdentate complex still exhibits a higher quantum yield than the bidentate material, and the spectral color purity of the former is substantially superior even in this more rigid medium.

The average radiative decay rate of Pt(4,6-dFdpyb)Cl at ambient temperature (1.2×10^5 s^{-1}) is significantly lower than the values reported for many Ir(III) compounds (up to 7×10^5 s^{-1})[11,13,79−82] because of generally less efficient SOC in square-planar complexes as compared to octahedrally coordinated materials.[13,41,78] Nevertheless, the terdentate Pt(II) compound with its high quantum yield at 300 K represents a very interesting blue-light emitting OLED material. In particular, the strategy to increase the molecular rigidity in Pt(4,6-dFdpyb)Cl has proven to be very successful in reducing the intensities of the vibrational satellite bands in the green spectral range. As a consequence, a remarkable improvement of the color purity with respect to blue emission as compared to the less rigid Pt(4,6-dFppy)(acac) is achieved, even though the emitting triplet state of the latter compound lies at slightly higher energy.

These significant differences in photoluminescence between the bidentate and the terdentate complex also translate to the electroluminescence behavior. For example, OLEDs prepared using the two emitters, having otherwise identical device architectures, have been reported to display CIE coordinates of (0.24; 0.37) (**1**) and (0.18, 0.32) (**2**), respectively.[27,83] Moreover, the high color purity of **2**, with low contributions from the vibrational components in the green range of the spectrum, is retained in related terdentate complexes in which the emission is shifted yet further to the blue. Thus, introduction of electron-donating methoxy substituents into the pyridyl-4-position raises the excited state energy, leading to CIE coordinates of (0.18, 0.27) in a similarly constructed OLED;[84] an external quantum efficiency of 6.1% photons/electron has been reported in that case.[40]

In summary, this study has highlighted the potential benefits of using terdentate over bidentate ligands in the construction of OLED emitters offering high color purity. The results provide insight into the molecular origins of the differences between the two, which may guide the future design of efficiently emitting materials for light-emitting device applications.

AUTHOR INFORMATION

Corresponding Author

*E-mail: hartmut.yersin@chemie.uni-regensburg.de (H.Y.), j.a.g.williams@durham.ac.uk (J.A.G.W.).

ACKNOWLEDGMENTS

The Bundesministerium für Bildung und Forschung (BMBF) is gratefully acknowledged for providing the funding for this investigation. We thank the British Council and the German Academic Exchange Service (DAAD) for a bilateral ARC travel grant, the COST project for financial support within the project D35-0010-05, and the University of Durham for a doctoral fellowship to L.M. Prof. Dr. Mark E. Thompson (University of Southern California, Los Angeles) is acknowledged for a fruitful cooperation with respect to Pt(4,6-dFppy)(acac).

REFERENCES

(1) Yersin, H., Ed.; *Highly Efficient OLEDs with Phosphorescent Materials*; Wiley-VCH: Weinheim, Germany, 2008.
(2) Chou, P. T.; Chi, Y. *Chem.—Eur. J.* **2007**, *13*, 380.
(3) Kalinowski, J.; Fattori, V.; Cocchi, M.; Williams, J. A. G. *Coord. Chem. Rev.* **2011**, *255*, 2401.
(4) Evans, R. C.; Douglas, P.; Winscom, C. *Coord. Chem. Rev.* **2006**, *250*, 2093.
(5) Polikarpov, E.; Thompson, M. E. *Mater. Matters* **2007**, *2*, 21.
(6) Xiao, L.; Chen, Z.; Qu, B.; Luo, J.; Kong, S.; Gong, G.; Kido, J. *Adv. Mater.* **2011**, *23*, 926.
(7) Che, C.-M.; Kwok, C.-C.; Lai, S.-W.; Rausch, A. F.; Finkenzeller, W. J.; Zhu, N.; Yersin, H. *Chem.—Eur. J.* **2010**, *16*, 233.
(8) Baldo, M. A.; O'Brien, D. F.; Thompson, M. E.; Forrest, S. R. *Phys Rev. B* **1999**, *60*, 14422.
(9) Yersin, H. *Top. Curr. Chem.* **2004**, *241*, 1.
(10) Hung, L. S.; Chen, C. H. *Mater. Sci. Eng. R* **2002**, *39*, 143.
(11) Sajoto, T.; Djurovich, P. I.; Tamayo, A. B.; Oxgaard, J.; Goddard, W. A. III; Thompson, M. E. *J. Am. Chem. Soc.* **2009**, *131*, 9813.
(12) Yang, L.; Okuda, F.; Kobayashi, K.; Nozaki, K.; Tanabe, Y.; Ishii, Y.; Haga, M. A. *Inorg. Chem.* **2008**, *47*, 7154.
(13) Yersin, H.; Rausch, A. F.; Czerwieniec, R.; Hofbeck, T.; Fischer, T. *Coord. Chem. Rev.* **2011**, *255*, 2622.
(14) Treboux, G.; Mizukami, J.; Yabe, M.; Nakamura, S. *Chem. Lett.* **2007**, *36*, 1344.
(15) Williams, J. A. G. *Top. Curr. Chem.* **2007**, *281*, 205.
(16) Sajoto, T.; Djurovich, P. I.; Tamayo, A.; Yousufuddin, M.; Bau, R.; Thompson, M. E.; Holmes, R. J.; Forrest, S. R. *Inorg. Chem.* **2005**, *44*, 7992.
(17) Haneder, S.; Da Como, E.; Feldmann, J.; Lupton, J. M.; Lennartz, C.; Erk, P.; Fuchs, E.; Molt, O.; Münster, I.; Schildknecht, C.; Wagenblast, G. *Adv. Mater.* **2008**, *20*, 3325.
(18) Unger, Y.; Meyer, D.; Molt, O.; Schildknecht, C.; Münster, I.; Wagenblast, G.; Strassner, T. *Angew. Chem., Int. Ed.* **2010**, *49*, 10214.
(19) Lo, S.-C.; Harding, R. E.; Shipley, C. P.; Stevenson, S. G.; Burn, P. L.; Samuel, I. D. W. *J. Am. Chem. Soc.* **2009**, *131*, 16681.
(20) Chen, K.; Yang, C.-H.; Chi, Y.; Liu, C.-S.; Chang, C.-H.; Chen, C.-C.; Wu, C.-C.; Chung, M.-W.; Cheng, Y.-M.; Lee, G.-H.; Chou, P.-T. *Chem.—Eur. J.* **2010**, *16*, 4315.
(21) Lin, C.-H.; Chang, Y.-Y.; Hung, J.-Y.; Lin, C.-Y.; Chi, Y.; Chung, M.-W.; Lin, C.-L.; Chou, P.-T.; Lee, G.-H.; Chang, C.-H.; Lin, W. C. *Angew. Chem., Int. Ed.* **2011**, *50*, 3182.
(22) Eum, M.-S.; Chin, C. S.; Kim, S. Y.; Kim, C.; Kang, S. K.; Nam, H. H.; Seo, J. H.; Kim, G. Y.; Kim, Y. K. *Inorg. Chem.* **2008**, *47*, 6289.

(23) Di Censeo, D.; Fantacci, S.; De Angelis, F.; Klein, C.; Evans, N.; Kalyanasundaram, K.; Bolink, H. J.; Grätzel, M.; Nazeeruddin, M. K. *Inorg. Chem.* **2008**, *47*, 980.
(24) Rausch, A. F.; Monkowius, U.; Zabel, M.; Yersin, H. *Inorg. Chem.* **2010**, *49*, 7818.
(25) Li, J.; Djurovich, P. I.; Alleyne, B. D.; Tsyba, I.; Ho, N. N.; Bau, R.; Thompson, M. E. *Polyhedron* **2004**, *23*, 419.
(26) Czerwieniec, R.; Yu, J.; Yersin, H. *Inorg. Chem.* **2011**, *50*, 8293.
(27) Yang, X.; Wang, Z.; Madakuni, S.; Li, J.; Jabbour, G. E. *Adv. Mater.* **2008**, *20*, 2405.
(28) Brooks, J.; Babayan, Y.; Lamansky, S.; Djurovich, P. I.; Tsyba, I.; Bau, R.; Thompson, M. E. *Inorg. Chem.* **2002**, *41*, 3055.
(29) Cocchi, M.; Kalinowski, J.; Fattori, V.; Williams, J. A. G.; Murphy, L. *Appl. Phys. Lett.* **2009**, *94*, 073309.
(30) Pettijohn, C. N.; Jochnowitz, E. B.; Chuong, B.; Nagle, J. K.; Vogler, A. *Coord. Chem. Rev.* **1998**, *171*, 85.
(31) Farley, S. J.; Rochester, D. L.; Thompson, A. L.; Howard, J. A. K.; Williams, J. A. G. *Inorg. Chem.* **2005**, *44*, 9690.
(32) Ma, B.; Djurovich, P. I.; Thompson, M. E. *Coord. Chem. Rev.* **2005**, *249*, 1501.
(33) Gliemann, G.; Yersin, H. *Struct. Bonding (Berlin)* **1985**, *62*, 87.
(34) Lai, S.-W.; Chan, M. C.-W.; Cheung, T.-C.; Peng, S.-M.; Che, C.-M. *Inorg. Chem.* **1999**, *38*, 4046.
(35) Yersin, H.; Donges, D.; Humbs, W.; Strasser, J.; Sitters, R.; Glasbeek, M. *Inorg. Chem.* **2002**, *41*, 4915.
(36) Mdleleni, M. M.; Bridgewater, J. S.; Watts, R. J.; Ford, P. C. *Inorg. Chem.* **1995**, *34*, 2334.
(37) Adamovich, V.; Brooks, J.; Tamayo, A.; Alexander, A. M.; Djurovich, P. I.; D'Andrade, B. W.; Adachi, C.; Forrest, S. R.; Thompson, M. E. *New J. Chem.* **2002**, *26*, 1171.
(38) D'Andrade, B. W.; Forrest, S. R. *J. Appl. Phys.* **2003**, *94*, 3101.
(39) Mroz, W.; Botta, C.; Giovanella, U.; Rossi, E.; Colombo, A.; Dragonetti, C.; Roberto, D.; Ugo, R.; Valore, A.; Williams, J. A. G. *J. Mater. Chem.* **2011**, *21*, 8653.
(40) Cocchi, M.; Kalinowski, J.; Murphy, L.; Williams, J. A. G.; Fattori, V. *Org. Electron.* **2010**, *11*, 388.
(41) Rausch, A. F.; Homeier, H. H. H.; Yersin, H. *Top. Organomet. Chem.* **2010**, *29*, 193.
(42) Rausch, A. F.; Thompson, M. E.; Yersin, H. *Chem. Phys. Lett.* **2009**, *468*, 46.
(43) Rausch, A. F.; Yersin, H. *Chem. Phys. Lett.* **2010**, *484*, 261.
(44) Williams, J. A. G.; Beeby, A.; Davies, E. S.; Weinstein, J. A.; Wilson, C. *Inorg. Chem.* **2003**, *42*, 8609.
(45) Rausch, A. F.; Murphy, L.; Williams, J. A. G.; Yersin, H. *Inorg. Chem.* **2009**, *48*, 11407.
(46) Wang, Z.; Turner, E.; Mahoney, V.; Madakuni, S.; Groy, T.; Li, J. *Inorg. Chem.* **2010**, *49*, 11276.
(47) Sotoyama, W.; Satoh, T.; Sato, H.; Matsuura, A.; Sawatari, N. *J. Phys. Chem. A* **2005**, *109*, 9760.
(48) Tong, G. S.-M.; Che, C.-M. *Chem.—Eur. J.* **2009**, *15*, 7225.
(49) Shi, L. L.; Li, T.; Zhao, S. S.; Li, H.; Su, Z. *Theor. Chem. Acc.* **2009**, *124*, 29.
(50) Williams, J. A. G.; Develay, S.; Rochester, D. L.; Murphy, L. *Coord. Chem. Rev.* **2008**, *252*, 2596.
(51) Cocchi, M.; Virgili, D.; Fattori, V.; Rochester, D. L.; Williams, J. A. G. *Adv. Funct. Mater.* **2007**, *17*, 285.
(52) Evans, R. C.; Douglas, P.; Williams, J. A. G.; Rochester, D. L. J. *Fluorescence* **2006**, *16*, 201.
(53) Rochester, D. L.; Develay, S.; Záliš, S.; Williams, J. A. G. *Dalton Trans.* **2009**, *10*, 1728.
(54) Botchway, S. W.; Charnley, M.; Haycock, J. W.; Parker, A. W.; Rochester, D. L.; Weinstein, J. A.; Williams, J. A. G. *Proc. Natl. Acad. Sci. U.S.A.* **2008**, *105*, 16071.
(55) Smith, T.; Guild, J. *Trans. Opt. Soc.* **1931/32**, *33*, 73.
(56) To the best of our knowledge, no crystal structure data for Pt(4,6-dFppy)(acac) are available. However, it can be expected that the Pt-C distance closely resembles that reported for comparable compounds, compare refs 24, 36; Chassot, L.; Müller, E.; von Zelewsky, A. *Inorg. Chem.* **1984**, *23*, 4249.
(57) Maruszewski, K.; Strommen., D. P.; Kincaid, J. R. *J. Am. Chem. Soc.* **1993**, *115*, 8345.
(58) Danielsson, E.; Lumpkin, R. S.; Meyer, T. J. *J. Phys. Chem.* **1987**, *81*, 1305.
(59) Thompson, D. W.; Fleming, C. N.; Myron, B. D.; Meyer, T. J. *J. Phys. Chem. B* **2007**, *111*, 6930.
(60) Yersin, H.; Finkenzeller, W. J. In *Highly Efficient OLEDs with Phosphorescent Materials*; Yersin, H., Ed.; Wiley-VCH: Weinheim, Germany, 2008; p 1.
(61) Yersin, H.; Humbs, W.; Strasser, J. *Top. Curr. Chem.* **1997**, *191*, 153.
(62) Yersin, H.; Donges, D. *Top. Curr. Chem.* **2001**, *214*, 81.
(63) Shpol'skii, E. V. *Sov. Phys. Usp. (Engl. Transl.)* **1960**, *3*, 372.
(64) Friedrich, J.; Haarer, D. *Angew. Chem., Int. Ed.* **1984**, *23*, 113.
(65) Becker, D.; Yersin, H.; von Zelewsky, A. *Chem. Phys. Lett.* **1995**, *235*, 490.
(66) Kober, E. M.; Caspar, J. V.; Lumpkin, R. S.; Meyer, T. J. *J. Phys. Chem.* **1986**, *90*, 3722.
(67) Colombo, M. G.; Hauser, A.; Güdel, H. U. *Inorg. Chem.* **1993**, *32*, 3088.
(68) Mallick, P. K.; Danzer, G. D.; Strommen, D. P.; Kincaid, J. R. *J. Phys. Chem.* **1988**, *92*, 5628.
(69) Solomon, E. I. *Comments Inorg. Chem.* **1984**, *3*, 225.
(70) Henderson, B.; Imbusch, G. F. *Optical Spectroscopy of Inorganic Solids*; Clarendon: Oxford, 1989.
(71) Seiler, R.; Kensy, U.; Dick, B. *Phys. Chem. Chem. Phys.* **2001**, *3*, 5373.
(72) van de Streek, J.; Verwer, P.; Bennema, P.; Vlieg, E. *Acta Crystallogr., Sect. B* **2002**, *58*, 677.
(73) Finkenzeller, W. J.; Yersin, H. *Chem. Phys. Lett.* **2003**, *377*, 299.
(74) Azumi, T.; O'Donnell, C. M.; McGlynn, S. P. *J. Chem. Phys.* **1966**, *45*, 2735.
(75) Harrigan, R. W.; Crosby, G. A. *J. Chem. Phys.* **1973**, *59*, 3468.
(76) The splitting between the T_1 substates II and III of Pt(4,6-dFppy)(acac) is smaller than 1 cm^{-1}; therefore, a simplified two-level-function was used, applying only one averaged decay time for these two substates.
(77) Miki, H.; Shimada, M.; Azumi, T.; Brozik, J. A.; Crosby, G. A. *J. Phys. Chem.* **1993**, *97*, 11175.
(78) Rausch, A. F.; Homeier, H. H. H.; Djurovich, P. I.; Thompson, M. E.; Yersin, H. *Proc. SPIE* **2007**, *6655*, 66550F.
(79) Rausch, A. F.; Thompson, M. E.; Yersin, H. *Inorg. Chem.* **2009**, *48*, 1928.
(80) Rausch, A. F.; Thompson, M. E.; Yersin, H. *J. Phys. Chem. A* **2009**, *113*, 5927.
(81) Williams, J. A. G.; Wilkinson, A. J.; Whittle, V. L. *Dalton Trans.* **2008**, 2081.
(82) Hofbeck, T.; Yersin, H. *Inorg. Chem.* **2010**, *49*, 9290.
(83) Device structure = ITO/PEDOT:PSS/TCTA/26mCPy:**Pt**(2%)/BCP/CsF/Al, where **Pt** represents the Pt complex **1** or **2**; PEDOT:PSS = poly(3,4-ethylenedioxythiophene):poly(styrenesulfonate); TCTA = 4,4′,4″-tris(*N*-carbazolyl)triphenylamine; 26mCPy = 2,6-bis(*N*-carbazolyl)pyridine; BCP = 2,9-dimethyl-4,7-diphenyl-1,10-phenanthroline (see reference 27). Note that the CIE coordinates depend on the environment of the emitter: compare Table 1 and ref 27.
(84) Device structure = ITO/TPD:PC(3:1)/TCTA/TCTA:**Pt**(5%)/TAZ/LiF/Al, where **Pt** represents the Pt(II) complex platinum N^C$_2$^N-[1,3-di(4-methoxy-pyryd-2-yl)-4,6 difluorobenzene] chloride; TPD = *N*,*N*′-diphenyl-*N*,*N*′-bis(3-methyl)-1,1′-biphenyl-4,4′-diamine; PC = poly carbonate; TAZ = 3-phenyl-4-(1′-naphthyl)-5-phenyl-1,2,4-triazole (see ref 40).